Smoothly Connected Preemptive Impact Reduction and Contact Impedance Control

Hikaru Arita, *Member, IEEE*, Hayato Nakamura, Takuto Fujiki, and Kenji Tahara, *Member, IEEE*

***Abstract*—This article proposes novel control methods that lower impact force by preemptive movement and smooth transition to conventional contact-based impedance control. These techniques are suggested for application in force-control-based robots and position/velocity-control-based robots. Strong impact forces have a negative influence on multiple robotic tasks. Recently, preemptive impact reduction techniques that expand conventional contact impedance control using proximity sensors have been examined. However, a seamless transition from impact reduction to contact impedance control has yet to be demonstrated. It has, therefore, been necessary to switch control strategies or perform complicated parameter tuning. In contrast, our proposed methods utilize a serial combined impedance control framework to solve these problems. The preemptive impact reduction feature can be added to an already-implemented impedance controller because the parameter design is divided into impact reduction and contact impedance control. There is no discontinuity or abrupt alteration in the contact force, nor are there any excessively large contact forces that exceed the intended repulsive force established by the contact impedance control during the transition. Furthermore, although the preemptive impact reduction uses a crude optical proximity sensor, the influence of reflectance is minimized by employing a virtual viscous force. Analyses and real-world experiments with a 1-D mass model confirm these features, which are useful for many robots performing contact tasks.**

***Index Terms*—Contact transition, impact reduction, optical proximity sensor, sensor-based reactive control.**

I. Introduction

A. Background

THE majority of robots manage transitions between contact and noncontact states. Touching a robot hand to an object, landing or takeoff of legged or aerial robots, and collisions between a human or an environment and cooperative or mobile robots are examples of such transitions. However, handling these transitions is known to be one of the challenging problems in robotics. Its difficulties can be classified into two topics. One is that the physical constraint changes dramatically during the transition, i.e., the robot's equation of motion is switched. This phenomenon may make the robot go out of control. The second is that an impact force is generated during the noncontact-to-contact transition. Usually, this impact force is significantly large and, thus, dangerous. It may, for example, cause the robot and the environment to be damaged, cause a robot's hand to fail to grasp, induce a flick, knock a legged robot down, and destabilize the robot control.

Typical conventional impact reduction methods use soft materials or force control, with soft materials being the standard approach [1], [2], [3]. Because of their flexibility, soft materials can absorb impact. However, a massive absorbed force may cause a robot to oscillate. Moreover, flexibility complicates accurate control, as mentioned in [4]. Despite active research in the field of soft robotics, these are difficult problems without established solutions.

Force control has long been studied and is well known. In particular, impedance control is practically used for manipulation, locomotion, and many other tasks [5], [6], [7], [8], [9], [10]. Impedance control can reduce impact by setting parameters to make the desired impedance soft, and it can also perform dexterous tasks by making the desired impedance hard. However, the efficacy of impact reduction through force control is limited due to the finite response speed. In other words, the reduction method fails to execute fast enough for impulsive forces with a frequency higher than the response frequency.

Preemptive impact reduction methods have recently been developed [11], [12]. These methods use proximity sensors mounted near the contact area and are based on impedance control. The proximity sensors are short-range external sensors. Compared to other types, optical proximity sensors have small sizes and fast responses [13]. They are often attached to feet in these methods; moreover, the outputs are used to calculate virtual forces that serve as impedance control inputs. The virtual force input alleviates the problems mentioned above with classical impedance control and achieves high effects for impact reduction. In these methods, however, an impedance control strategy works for both impact reduction and contact force control, i.e., these tasks interfere with each other. Consequently, selecting parameters that consider overall performance [11] or switching between virtual and contact forces [12] is needed. The former introduces a tradeoff between impact reduction and contact force control performances, and the latter destabilizes the system as

Manuscript received 7 December 2022; revised 17 April 2023; accepted 2 June 2023. Date of publication 30 June 2023; date of current version 4 October 2023. This work was supported in part by Japan Society for the Promotion of Science Grants-in-Aid for Scientific Research under Grant JP20K14702. This article was recommended for publication by Associate Editor Alexander Dietrich and Editor Mark Yim upon evaluation of the reviewers' comments. *(Corresponding author: Hikaru Arita.)*

Hikaru Arita, Hayato Nakamura, and Kenji Tahara are with the Department of Mechanical Engineering, Kyushu University, Fukuoka 819-0395, Japan (e-mail: arita@ieee.org; nakamura@hcr.mech.kyushu-u.ac.jp; tahara@ieee.org).

Takuto Fujiki was with the Department of Mechanical Engineering, Kyushu University, Fukuoka 819-0395, Japan. He is now with Yaskawa Electric Corporation, Fukuoka 806-0004, Japan (e-mail: fujiki@hcr.mech.kyushu-u.ac.jp).

Color versions of one or more figures in this article are available at https://doi.org/10.1109/TRO.2023.3286045.

Digital Object Identifier 10.1109/TRO.2023.3286045

with other switching methods. The above transition between proximity and contact is listed in [13] as one of the problems garnering attention in the proximity perception field.

This study proposes novel control methods that perform preemptive impact reduction and contact force control. The control parameters are categorized based on their association with the functionality of preemptive impact reduction and contact force control. It is feasible to design these parameters independently. The transition from impact reduction to contact force control is smooth. There is no switching of inputs and control strategies. The proposed techniques will improve the robotic performances of running, jumping, and other dynamic activities that have been limited thus far due to avoiding potential damage caused by improperly handled impact forces. These techniques will also facilitate delicate tasks, such as grasping fragile objects and human interaction. More specific characteristics of the proposed methods are highlighted in the following section compared to related works.

B. Related Works

1) (Contact) Impedance Control: Impedance control is clustered into a force-control-based type and a position/velocity-control-based type. Force-control-based impedance control [14] is simply denoted as "impedance control," which calculates the force command based on the controlled object's position, velocity, and acceleration. The controlled object is referred to as the "plant" in this study. Position/velocity-control-based impedance control [15] is called "admittance control." The position, velocity, and acceleration of a virtual object are calculated from a force input in admittance control, and the virtual object is tracked by the position/velocity controller. Although both controls aim to change the plant's dynamic behavior to the desired one, their characteristics differ. As the movement due to contact force is the input into impedance control, adequate backdrivability is needed. Furthermore, because impedance control uses a dynamic plant model to cancel itself through compensation, such as a computed torque method, model errors, notably friction, have an influence on performance, particularly positional accuracy. Admittance control does not require high backdrivability because it collects information about contact force with a force sensor, and the high-gain position/velocity controller provides high positional accuracy. However, no movement is generated by the force applied to the area without a sensor. Moreover, dramatically moving the virtual object because of a large contact force causes the system to become unstable.

Certain combined impedance and admittance controllers are proposed to incorporate the benefits of both. Ott et al. [16] presented a parallel combined controller that, depending on the situation, switches between admittance and impedance control. However, the method requires the environmental information to switch; furthermore, a controller switchover generally causes unstable behavior. Fujiki and Tahara [17] developed a serial combined controller. The admittance control part's calculated virtual object state is used as the impedance control part's equilibrium state. The serial combined controller achieves higher stability than admittance control and higher positional accuracy than impedance control. Our study employed the serial combined controller shown in [17] with generalization to achieve two distinct functions (preemptive impact reduction and contact impedance control) that demonstrate the desired characteristics within a single control strategy.

2) Noncontact/Virtual/Preemptive Impedance Control: Tsuji and Kaneko [18] proposed an early method for calculating virtual force from a noncontact sensor output and extending conventional impedance control to the noncontact region. Their method uses a vision sensor. A similar method is used in [19] to avoid collisions.

Because optical proximity sensors are small, have fast responses, and can actively use reflection, they have been used for impact reduction without occlusion. Virtual force calculated from the proximity sensor's output was introduced in [20]. The virtual force is an elastic force because its output depends on its distance from an object.

Sato et al. [11] proposed an impact reduction method using the virtual elastic force for legged robots. Their sensor was developed in such a manner that the virtual elastic force did not interfere with posture control after landing. The control parameters were tuned by trial and error to maximize an index that included impact reduction and posture control performances. Because the control parameters influenced both impact reduction and posture control performances, tuning is complex, and there is a tradeoff. Compared to [11], our proposed method enables us to distinctly delineate preemptive and postcontact actions. This separation simplifies the controller design process for a given task.

Guadarrama-Olvera et al. [12] proposed a method for using virtual elastic force as an input to a humanoid admittance controller. By calculating a virtual wrench from a virtual elastic force, the method reduces impact and maximizes the landing contact area. The virtual wrench is switched OFF after landing to prevent adding disturbance to the balance controller. However, parameter tuning considering the virtual wrench is not described. They also discussed that achieving a smooth transition between virtual impedance control and conventional contact impedance control would help improve walking stability. Work in [12] and our study are, therefore, linked in that our method attains a smooth transition, which is characterized as a desirable attribute in [12]. The results of analytical verification and experimental evaluation demonstrate an example of the seamless transition property.

3) Proximity-Sensor-Based Control: Many methods using proximity sensors are based on factors other than impedance control replacing contact forces with virtual forces. Some of these techniques are also relevant to this study's proposed method. The method proposed by Koyama et al. [21] is particularly relevant, as it uses virtual viscous forces to slow the robot finger before contact. The derivative of the distance output from the customized optical proximity sensor is used to calculate the virtual viscous force. The virtual viscous force can be derived from the output ratio of a primitive optical proximity sensor. Koyama et al. [22] demonstrated that the output ratio is not affected by reflectance. In [22], their output ratio calculation

estimates the time to contact for grasping with the robot finger. Both the methods in [21] and [22] stop the robot after contact. As with other position/velocity-based controls, switching is required if contact force control is to be performed. For impact reduction, the proposed method in this study employs the virtual viscous force derived from the output ratio of a primitive optical proximity sensor.

The method proposed by Arita and Suzuki [23] uses proximity sensors with force control. To execute their desired transition between noncontact and contact, they employed a virtual elastic force and changed its magnitude by controlling the proximity sensor's emitting light. Although the method demonstrated smooth transition capability, the desired contact force was constant, and the design of the desired force still requires further investigation. The contact force property of the method proposed here can be designed similarly to conventional impedance control.

Ding and Thomas [24] proposed a method for adaptive parameter tuning of contact impedance control using proximity sensor outputs. This method can prepare in advance for collisions that the collision avoidance function of [25] cannot entirely avoid. Because [24] aims to propose the preparation method, the transition between the collision avoidance feature and the preparation method is not mentioned, and impact forces are not evaluated. In the future, the adaptive tuning method could be combined with the method proposed in this article to improve the positional accuracy of the impedance control part.

C. Contents of This Article

The contribution of this article is proposing a novel control method to achieve impact reduction and contact impedance control with the following characteristics.

1) The proposed method can be applied to a multitude of robots. The proposed approach can be employed by both force-controlled and position/velocity-control-based robots. Although the method requires an optical reflective proximity sensor, the sensor is compact and easy to implement.
2) The method does not require detailed information about the environment/object. Despite the usual susceptibility of the optical reflective sensor to reflectance, the effect of reflectance on the proposed method is minimal because of the integrated use of virtual viscous force and the control framework.
3) The technique attains seamless contact transition, wherein no abrupt or sizable contact force is encountered during the shift from noncontact to contact states. The preemptive impact reduction function significantly alleviates the impact force. Despite accomplishing the two functions above, the method does not switch control laws.
4) The method can use the traditional knowledge of impedance control. Although the proposed method combines preemptive impact reduction and contact impedance control into a single control law, the control parameters associated with each function are categorized. Notably, the contact impedance control after established contact is the same as the usual one, and therefore, the control parameters can be reused.

The rest of this article is organized as follows. Section II introduces the proposed method for force-control-based robots. In Sections II–IV, the method for force-control-based robots is utilized for demonstration, as it can be naturally derived from [17]. The method for position/velocity-based robots is described in Section V. This study employs a one-dimensional (1-D) mass model, which is suitable for discussing collisions because they are essentially 1-D phenomena. As an example, the results of this study can be directly applied to more sophisticated robotic systems, such as serial-linked arms, robot hands, or legged robots, by substituting the approaching direction's impedance control in the task space with the proposed method. Section III analyzes the proposed method and demonstrates the theoretical independence of reflectance, divided design, and smooth transition. Section IV evaluates the proposed method in actual experiments. Section V contains the expansions, which include the proposed method for position/velocity-control-based robots and the generalized controller. Section VI describes the discussion of benefits, limitations, and future works. Finally, Section VII concludes this article.

II. Proposed Controller for Force-Control-Based Robots

Fig. 1 shows the block diagram of the proposed controller for force-control-based robots. The primary differences between [17] are that the forces in the impedance and admittance control parts are distinguished, and the force in the admittance control part is derived from the proximity sensor output. This section briefly introduces the controller. The details are analyzed in the next section.

The trajectory planner determines the plant's desired state $(x_{\mathrm{d}}, \dot{x}_{\mathrm{d}}, \ddot{x}_{\mathrm{d}})$. Because the planner should be designed specifically for a given task, it is not the focus of this study.

A primitive optical reflective proximity sensor is used as the proximity sensor in Fig. 1. The minimum necessary components are an LED, a phototransistor, and two resistors. The phototransistor generates the sensor output by receiving lights emitted by the LED and reflected at the surface of a detected object.

The virtual force generator in this study outputs the virtual viscous force f_{p}. The equation is

$$f_{\mathrm{p}} = G_{\mathrm{p}} \frac{\dot{\xi}}{\xi} \tag{1}$$

where ξ is the proximity sensor output and G_{p} is the scale coefficient for the sensor output. The subscript "p" indicates that it is related to the proximity sensor. The correlation between ξ and the distance from the sensor to an obstacle is explicated in Section III-A.

The admittance control part simulates the virtual object affected by f_{p} with the following equation of motion:

$$M_{\mathrm{a}}(\ddot{x}_{\mathrm{v}} - \ddot{x}_{\mathrm{d}}) + D_{\mathrm{a}}(\dot{x}_{\mathrm{v}} - \dot{x}_{\mathrm{d}}) + K_{\mathrm{a}}(x_{\mathrm{v}} - x_{\mathrm{d}}) = f_{\mathrm{p}} \tag{2}$$

where M_{a}, D_{a}, and K_{a} are the desired inertia, viscosity, and stiffness of the admittance control part, respectively, and $(x_{\mathrm{v}}, \dot{x}_{\mathrm{v}}, \ddot{x}_{\mathrm{v}})$

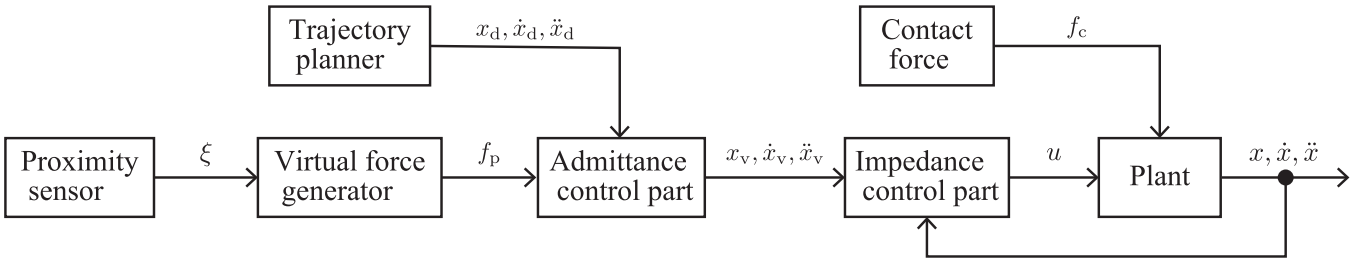

Fig. 1. Block diagram of the proposed controller for force-control-based robots. Serial combining admittance control and impedance control parts construct the controller. The unique point is that the force received by the admittance control part is not a contact force but a virtual force.

is the virtual object's state. In conventional admittance control, the calculated state of the virtual object is tracked with a position/velocity controller. In contrast, the control framework proposed in [17] employed impedance control for tracking.

The impedance control part changes the dynamic behavior of the plant to the desired behavior. The virtual object's state equals the equilibrium state of the desired dynamic behavior. The plant's equation of motion is assumed as follows in this study:

$$m\ddot{x} = u + f_c \tag{3}$$

where m denotes the mass of the plant, x denotes its position, u denotes the controller's input force, and f_c denotes the contact force from an external environment or obstacle. In this case, u is given as follows:

$$u = \left(\frac{m}{M_i} - 1\right) f_c + m\ddot{x}_v - \frac{m}{M_i}\left[D_i(\dot{x} - \dot{x}_v) + K_i(x - x_v)\right] \tag{4}$$

where M_i, D_i, and K_i represent the desired inertia, viscosity, and stiffness of the impedance control part, respectively. The plant's motion equation is modified by substituting (4) into (3):

$$M_i(\ddot{x} - \ddot{x}_v) + D_i(\dot{x} - \dot{x}_v) + K_i(x - x_v) = f_c. \tag{5}$$

Even if the plant's model (3) is complicated, (5) can be obtained by adding compensation terms to (4) as long as the relevant model is provided.

f_p influences plant behavior via the virtual object's state.

III. Analysis for Force-Control-Based Robots

A. Independence of Reflectance

This section shows that (1) is, in theory, independent of reflectance. A similar description is given in [22].

The output of an optical reflective proximity sensor ξ can be modeled as follows:

$$\xi = G_\xi \frac{\alpha\psi}{(d + d_o)^n} \tag{6}$$

where G_ξ is the transform coefficient of the sensing element, such as a phototransistor, α is the detecting object's reflectance, ψ is the energy of the light emitted from the LED, d is the distance between the proximity sensor and the object, d_o is the offset distance to prevent direct contact between the electric components and the object, and n is the diffusion coefficient fixed by the sensor design. Only d is time varying. f_p can be rewritten by substituting (6) into (1) as

$$f_p = -\frac{G_p n}{d + d_o}\dot{d}. \tag{7}$$

As per (7), f_p is independent of α, is proportional to $\dot{d}$, and is inversely proportional to d. Therefore, f_p can be considered as a nonlinear virtual viscous force independent of reflectance. When in contact, $f_p = 0$ because $\dot{d} = 0$ and the denominator is d_o.

B. Divided Design

This section introduces that the parameters for impact reduction and contact impedance control are divided. The Laplace transform is used in analysis in this section.

The Laplace transform of (2) is as follows:

$$(s^2 M_a + sD_a + K_a)(X_v - X_d) = F_p \tag{8}$$

where $X_v = \mathcal{L}[x_v]$, $X_d = \mathcal{L}[x_d]$, and $F_p = \mathcal{L}[f_p]$. The following equation is obtained by solving (8) for X_v:

$$X_v = X_d + \frac{1}{s^2 M_a + sD_a + K_a} F_p. \tag{9}$$

Similarly, solving (5) for x's Laplace transform serves the following equation:

$$X = X_v + \frac{1}{s^2 M_i + sD_i + K_i} F_c \tag{10}$$

where $X = \mathcal{L}[x]$ and $F_c = \mathcal{L}[f_c]$. Eventually, X is represented by substituting (9) into (10) as

$$X = X_d + \frac{1}{s^2 M_a + sD_a + K_a} F_p + \frac{1}{s^2 M_i + sD_i + K_i} F_c. \tag{11}$$

As per (11), the influence on the plant's movement of f_p is determined only by the parameters of the admittance control part, whereas the influence of f_c is determined only by the parameters of the impedance control part.

C. Smooth Transition

This section describes how selecting appropriate parameters results in the contact force immediately after the contact smoothly increases, and finally, contact impedance defined by the impedance control part is enabled.

Let $y = x_\mathrm{v} - x_\mathrm{d}$. When in contact, (2) can be expressed as follows because $f_\mathrm{p} = 0$, as described in Section III-A:

$$\ddot{y} + 2\zeta_\mathrm{a}\omega_\mathrm{a}\dot{y} + \omega_\mathrm{a}^2 y = 0 \tag{12}$$

where $\zeta_\mathrm{a} = D_\mathrm{a}/[2(M_\mathrm{a}K_\mathrm{a})^{1/2}]$ and $\omega_\mathrm{a} = (K_\mathrm{a}/M_\mathrm{a})^{1/2}$. Let t be the time from the contact. If $\zeta_\mathrm{a} = 1$, the general solution of (12) is given as

$$y = (\eta t + \sigma)\exp(-\omega_a t) \tag{13}$$

where $\eta = \nu + \omega_\mathrm{a}\sigma$, $\sigma = y(0) = x_\mathrm{v}(0) - x_\mathrm{d}(0)$, and $\nu = \dot{y}(0) = \dot{x}_\mathrm{v}(0) - \dot{x}_\mathrm{d}(0)$. Note that $\zeta_\mathrm{a} = 1$ means (2) is critical damping. Equation (2) determines the plant's movement after contact if $f_\mathrm{c} = 0$ and transition property immediately after contact if $f_\mathrm{c} \neq 0$. Critical damping is appropriate for (2) because it has the fastest convergence without oscillation. The transition property is further explained as follows.

The time derivatives of (13) are as follows:

$$\dot{y} = (-\omega_\mathrm{a}\eta t + \nu)\exp(-\omega_\mathrm{a} t) \tag{14}$$

$$\ddot{y} = \left[\omega_\mathrm{a}^2\eta t - \omega_\mathrm{a}(\eta + \nu)\right]\exp(-\omega_\mathrm{a} t). \tag{15}$$

From (5) and (13)–(15), the following equation is derived:

$$\begin{aligned} f_\mathrm{c} = {} & M_\mathrm{i}(\ddot{x} - \ddot{x}_\mathrm{d}) + D_\mathrm{i}(\dot{x} - \dot{x}_\mathrm{d}) + K_\mathrm{i}(x - x_\mathrm{d}) \\ & + \exp(-\omega_\mathrm{a} t)\{-\left[M_\mathrm{i}\omega_\mathrm{a}^2 - D_\mathrm{i}\omega_\mathrm{a} + K_\mathrm{i}\right]\eta t \\ & + [M_\mathrm{i}\omega_\mathrm{a}(\eta + \nu) - D_\mathrm{i}\nu - K_\mathrm{i}\sigma]\}. \end{aligned} \tag{16}$$

The initial contact force $f_\mathrm{c}(0)$ is determined by substituting $t = 0$ into (16) as

$$f_\mathrm{c}(0) = M_\mathrm{i}(a_\mathrm{c} - \ddot{x}_\mathrm{d}(0)) + M_\mathrm{i}\omega_\mathrm{a}(\eta + \nu) \tag{17}$$

where $\ddot{x}(0) = \ddot{x}_\mathrm{v}(0) = a_\mathrm{c}$, $\dot{x}(0) = \dot{x}_\mathrm{v}(0) = v_\mathrm{c}$, and $x(0) = x_\mathrm{v}(0) = x_\mathrm{c}$. Note that the initial conditions assume that the tracking error caused by the impedance control part can be ignored until contact. Equation (10) demonstrates that this assumption is met; however, it is not strictly satisfied in the following analysis. Even so, the experimental results in Section IV show that the influence of the violating the assumption is negligible. The first term on the right-hand side of (17) is the inertial force determined by the impedance control part. The second term is affected by the initial position and velocity; even if the impact reduction is successful, the second term produces an undesirable contact force.

The undesirable term can be eliminated by modifying the impedance control part. u is redefined by removing $m\ddot{x}_\mathrm{v}$ from (4)

$$u = \left(\frac{m}{M_\mathrm{i}} - 1\right) f_\mathrm{c} - \frac{m}{M_\mathrm{i}}\left[D_\mathrm{i}(\dot{x} - \dot{x}_\mathrm{v}) + K_\mathrm{i}(x - x_\mathrm{v})\right]. \tag{18}$$

The modification changes (16) and (17) as follows:

$$\begin{aligned} f_\mathrm{c} = {} & M_\mathrm{i}\ddot{x} + D_\mathrm{i}(\dot{x} - \dot{x}_\mathrm{d}) + K_\mathrm{i}(x - x_\mathrm{d}) \\ & + \exp(-\omega_\mathrm{a} t)[(D_\mathrm{i}\omega_\mathrm{a} - K_\mathrm{i})\eta t - D_\mathrm{i}\nu - K_\mathrm{i}\sigma] \end{aligned} \tag{19}$$

$$f_\mathrm{c}(0) = M_\mathrm{i}a_\mathrm{c}. \tag{20}$$

M_i is frequently set to m in practice to avoid the difficulty of measuring the contact force f_c. In this case, the above equations vary as follows:

$$u = -D_\mathrm{i}(\dot{x} - \dot{x}_\mathrm{v}) - K_\mathrm{i}(x - x_\mathrm{v}) \tag{21}$$

$$\begin{aligned} f_\mathrm{c} = {} & m\ddot{x} + D_\mathrm{i}(\dot{x} - \dot{x}_\mathrm{d}) + K_\mathrm{i}(x - x_\mathrm{d}) \\ & + \exp(-\omega_\mathrm{a} t)[(D_\mathrm{i}\omega_\mathrm{a} - K_\mathrm{i})\eta t - D_\mathrm{i}\nu - K_\mathrm{i}\sigma] \end{aligned} \tag{22}$$

$$f_\mathrm{c}(0) = ma_\mathrm{c}. \tag{23}$$

The desired inertial force of the impedance control part is represented by the right-hand side of (20) and (23). In particular, (23) shows the originally dynamic behavior of the plant without control. Note that the delay exists because the eliminated $m\ddot{x}_\mathrm{v}$ is the feedforward term of (4). Because the notation conveys the meaning, the inertia defined by the impedance control part is represented as M_i in the following analysis.

Equation (19) is the sum of the desired equation of motion of conventional impedance control and the fourth term on the right-hand side. The fourth term is extracted from (19) as follows:

$$f_\mathrm{tra} := \exp(-\omega_\mathrm{a} t)[(D_\mathrm{i}\omega_\mathrm{a} - K_\mathrm{i})\eta t - D_\mathrm{i}\nu - K_\mathrm{i}\sigma]. \tag{24}$$

The initial and final values are

$$f_\mathrm{tra}(0) = -D_\mathrm{i}\nu - K_\mathrm{i}\sigma \tag{25}$$

$$f_\mathrm{tra}(\infty) = 0. \tag{26}$$

It is desirable that $f_\mathrm{tra}(0) < f_\mathrm{tra}(t) < f_\mathrm{tra}(\infty)$ or $f_\mathrm{tra}(\infty) < f_\mathrm{tra}(t) < f_\mathrm{tra}(0)$ is satisfied. However, as shown in Fig. 2, f_tra may exceed the range. The following section analyzes the extreme value of f_tra to identify the condition satisfying the above range.

Because the extreme value analysis includes the evaluation of inequalities, the initial state signs must be confirmed. The situations that are possible to occur are shown in Fig. 3. Fig. 3 shows the situation when an obstacle approaches the plant and the one when the plant approaches an obstacle. In each situation, σ, ν, and η have the same sign, and the analytical results of all

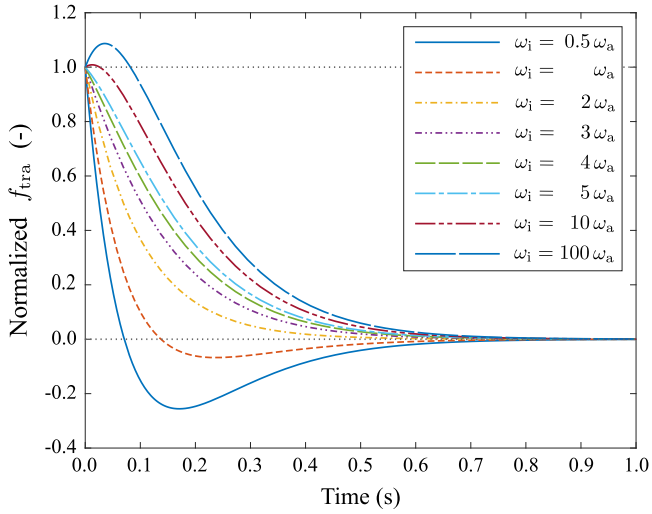

Fig. 2. Relation between the time from the contact and $f_\mathrm{tra}(t)/f_\mathrm{tra}(0)$ ($\sigma = 0.05, \nu = 0.3, \omega_\mathrm{a} = 10, \zeta_\mathrm{i} = 1$). Note that $f_\mathrm{tra}(0) < 0$. There are parameter conditions that have the local maximum or minimum value before convergence.

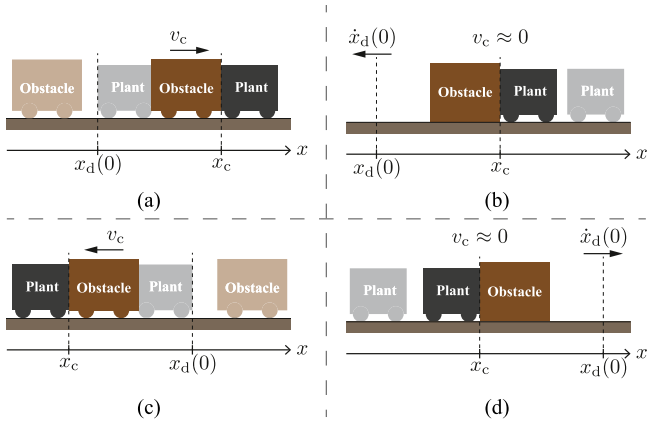

Fig. 3. Situations at the moment of contact. An obstacle approaches the plant in (a) and (c). The plant approaches an obstacle in (b) and (d). In (a) and (b), $\sigma > 0, \nu > 0, \eta > 0$. In (c) and (d), $\sigma < 0, \nu < 0, \eta < 0$.

the situations are equivalent. The signs of σ, ν, and η are positive in the following analysis.

The time derivatives of (24) are as follows:

$$\dot{f}_{\text{tra}} = \exp(-\omega_{\text{a}} t)[-\omega_{\text{a}}(D_{\text{i}}\omega_{\text{a}} - K_{\text{i}})\eta t + (D_{\text{i}}\omega_{\text{a}-K_{\text{i}}})\eta + \omega_{\text{a}}(D_{\text{i}}\nu + K_{\text{i}}\sigma)] \tag{27}$$

$$\ddot{f}_{\text{tra}} = \exp(-\omega_{\text{a}} t)\left[\omega_{\text{a}}^2(D_{\text{i}}\omega_{\text{a}} - K_{\text{i}})\eta t - 2\omega_{\text{a}}(D_{\text{i}}\omega_{\text{a}-K_{\text{i}}})\eta - \omega_{\text{a}}^2(D_{\text{i}}\nu + K_{\text{i}}\sigma)\right]. \tag{28}$$

Let t_{ex} be the time when $\dot{f}_{\text{tra}} = 0$. $t_{\text{ex}} = \infty$ or

$$t_{\text{ex}} = \frac{1}{\omega_{\text{a}}} + \frac{D_{\text{i}}\nu + K_{\text{i}}\sigma}{(D_{\text{i}}\omega_{\text{a}} - K_{\text{i}})\eta}. \tag{29}$$

The case when $t_{\text{ex}} = \infty$ is trivial. The case of (29) is analyzed as follows.

From (28) and (29), the following equation is obtained:

$$\ddot{f}_{\text{tra}}(t_{\text{ex}}) = -(D_{\text{i}}\omega_{\text{a}} - K_{\text{i}}) \times \omega_{\text{a}}\eta \exp\left(-1 - \frac{D_{\text{i}}\nu + K_{\text{i}}\sigma}{\omega_{\text{a}}(D_{\text{i}}\omega_{\text{a}} - K_{\text{i}})\eta}\right). \tag{30}$$

Because $\omega_{\text{a}} > 0$, $\eta > 0$, and $\exp(\cdot) > 0$, we have

$$\text{sgn}\left(\ddot{f}_{\text{tra}}(t_{\text{ex}})\right) = -\text{sgn}(D_{\text{i}}\omega_{\text{a}} - K_{\text{i}}). \tag{31}$$

From (31), f_{tra} has a local maximum value when $D_{\text{i}}\omega_{\text{a}} - K_{\text{i}} > 0$, i.e.,

$$\omega_{\text{i}} < 2\zeta_{\text{i}}\omega_{\text{a}} \tag{32}$$

where $\omega_i = (K_{\text{i}}/M_{\text{i}})^{1/2}$ and $\zeta_{\text{i}} = D_{\text{i}}/[2(M_{\text{i}}K_{\text{i}})^{1/2}]$. In this case, because the second term on the right-hand side of (29) is positive, t_{ex} is always positive. Consequently, if (32) is met, f_{tra} has a local maximum value after contact.

On the other hand, f_{tra} has a local minimum value when $D_{\text{i}}\omega_{\text{a}} - K_{\text{i}} < 0$, i.e.,

$$\omega_{\text{i}} > 2\zeta_{\text{i}}\omega_{\text{a}}. \tag{33}$$

Because the second term on the right-hand side of (29) is negative in this case, t_{ex} can be either positive or negative. If $t_{\text{ex}} < 0$, there is no local minimum value after contact. However, the parameter condition derived directly from $t_{\text{ex}} < 0$ clearly includes the initial states. In practice, these initial states are unknown when the parameter is designed. As a result, considering the contraposition, a sufficiency condition is derived below. The following equation is given by assuming $t_{\text{ex}} \geq 0$ as

$$t_{\text{ex}} = \frac{1}{\omega_{\text{a}}} + \frac{D_{\text{i}}\nu + K_{\text{i}}\sigma}{(D_{\text{i}}\omega_{\text{a}} - K_{\text{i}})\eta} = \frac{(D_{\text{i}}\omega_{\text{a}} - K_{\text{i}})\eta + \omega_{\text{a}}(D_{\text{i}}\nu + K_{\text{i}}\sigma)}{\omega_{\text{a}}(D_{\text{i}}\omega_{\text{a}} - K_{\text{i}})\eta} \geq 0. \tag{34}$$

Because $\omega_{\text{a}} > 0$, $\eta > 0$, and $D_{\text{i}}\omega_{\text{a}} - K_{\text{i}} < 0$, (34) signifies that

$$(D_{\text{i}}\omega_{\text{a}} - K_{\text{i}})\eta + \omega_{\text{a}}(D_{\text{i}}\nu + K_{\text{i}}\sigma) \leq 0. \tag{35}$$

Equation (35) can be deformed as follows since $\nu > 0$, $\omega_{\text{i}} > 0$, and $M_{\text{i}} > 0$:

$$4\zeta_{\text{i}}\omega_{\text{a}} - \omega_{\text{i}} \leq -\frac{2\zeta_{\text{i}}\omega_{\text{a}}^2\sigma}{\nu}. \tag{36}$$

Because the right-hand side of (36) is always negative, (36) proves that "if (33) is satisfied, $t_{\text{ex}} \geq 0$ indicates $4\zeta_{\text{i}}\omega_{\text{a}} - \omega_{\text{i}} < 0$, i.e., $\omega_{\text{i}} > 4\zeta_{\text{i}}\omega_{\text{a}}$." Therefore, the contraposition, i.e., "if (33) is satisfied, $\omega_{\text{i}} \leq 4\zeta_{\text{i}}\omega_{\text{a}}$ indicates $t_{\text{ex}} < 0$" is true.

Eventually, the parameter condition for the case where f_{tra} has neither a local maximum nor minimum value after contact is as follows:

$$2\zeta_{\text{i}}\omega_{\text{a}} < \omega_{\text{i}} \leq 4\zeta_{\text{i}}\omega_{\text{a}}. \tag{37}$$

Note that $\omega_{\text{i}} \leq 4\zeta_{\text{i}}\omega_{\text{a}}$ is a conservative condition. If the initial states are obtained, the necessary condition can be derived by directly solving $t_{\text{ex}} < 0$. This can be confirmed in Fig. 2.

The following equation given by deforming (37) is often helpful for design:

$$\frac{\omega_{\text{i}}}{4\zeta_{\text{i}}} \leq \omega_{\text{a}} < \frac{\omega_{\text{i}}}{2\zeta_{\text{i}}}. \tag{38}$$

Note that ω_{i} and ζ_{i} are based on the estimated m and are influenced by model errors in the impedance control part. The parameter design with a certain margin of tolerance is desirable.

IV. Experiments for Force-Control-Based Robots

A. Experimental Setup

Fig. 4 shows an overview of the experimental setup. The setup, which includes a proximity sensor, an obstruction, a force sensor for observation, a dual linear stage, and a real-time controller, is capable of realizing the scenarios in Fig. 3. The dual linear stage (SLP-15-300-D-M3-A3-SH, Nippon Pulse Motor Co., Ltd., Tokyo, Japan) can individually move two tables. The plant with the proximity sensor was placed on the left table in Fig. 4. The obstacle was created using the right table in Fig. 4. Two motor drivers (MADLT11SM, Panasonic Industry Company, Ltd., Osaka, Japan) each control one shaft motor. The motor driver has four modes (position/velocity/force/velocity&force). The velocity&force mode indicates that it can alternate between the velocity and force modes during operation. The obstacle was

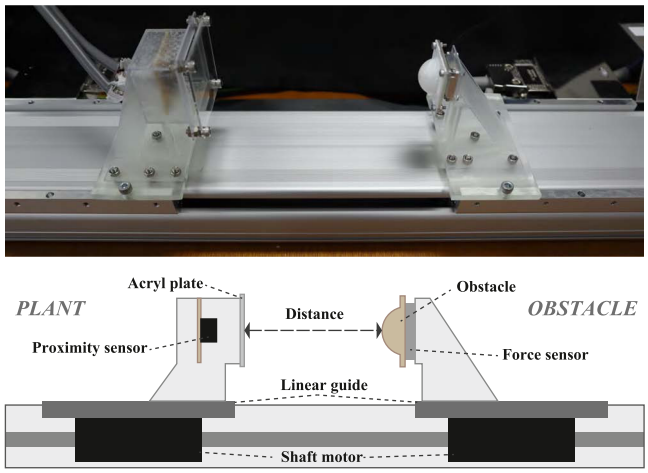

Fig. 4. Image and diagram of the experimental setup. The diagram is in the side view. The semitransparent parts are fixtures manufactured with a stereolithography printer.

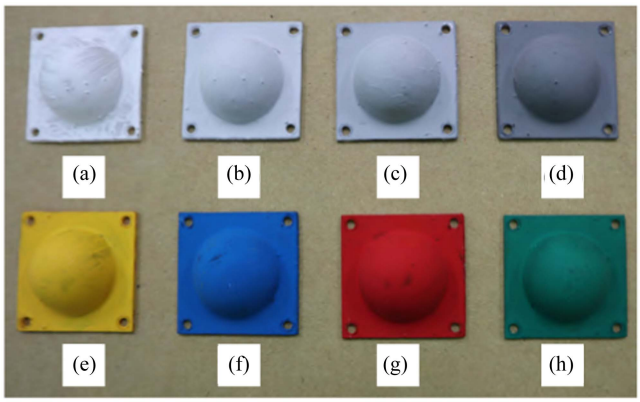

Fig. 5. Attachments of the obstacle's contact component. Their shapes are all the same, half-sphere. The description of each color is in Table I.

manipulated in the experiments using the velocity&force mode. These actuators and tables are connected by linear guides.

The force sensor (USL06-H5-50N-C and DSA-03A, Tec Gihan Co., Ltd., Ibaraki, Japan) was used only for measuring the contact force, rather than to control the plant. The proximity sensor is constructed by connecting three photo reflectors (RPR-220, ROHM Co., Ltd., Kyoto, Japan) in parallel, which improves the signal-to-noise ratio. There is no computational circuit in this rudimentary proximity sensor, which has an acrylic plate in front of it to prevent obstacles from getting closer than the focal distance or directly touching the sensing element. By calibrating the proximity sensor, the influence of the acrylic plate on the output was eliminated.

The obstacle's contact component can be replaced with other attachments, as shown in Fig. 5. These attachments are painted with acrylic paints (Acryl Gouache, Turner Colour Works Ltd., Osaka, Japan) in a variety of colors. Table I lists the names of the paints and colors used in this study. The obstacle is a half-sphere with a radius of 10 mm, placing the contact point and the proximity sensor's detected point on the force sensor's Z-axis.

TABLE I
OBSTACLE COLORS

Index in Fig. 5	Color name in this article	The paint's color name
(a)	White	WHITE
(b)	Gray1	NEUTRAL GRAY8
(c)	Gray2	NEUTRAL GRAY7
(d)	Gray3	NEUTRAL GRAY5
(e)	Red	PERMANENT RED
(f)	Blue	SKY BLUE
(g)	Yellow	PERMANENT LEMON
(h)	Green	PERMANENT GREEN MIDDLE

TABLE II
CONTROL PARAMETERS

Experiment	Impact reduction				Contact impedance		
	G_p	M_a	ω_a	ζ_a	m	ω_i	ζ_i
in Section IV-B	0.8	1	5	1	-	-	-
in Section IV-C					0.5	15	1

The real-time controller (MicroLabBox, dSPACE GmbH, Paderborn, Germany) measures the signal of the proximity sensor, force sensor, and encoder mounted in the dual linear stage and calculates the commands to the motor drivers. The control frequency is 1 kHz, whereas the measurement frequency of data for evaluation is 10 kHz. The noise on the proximity sensor's output is reduced using a fifth-order Butterworth low-path filter with a cutoff frequency of 500 Hz.

B. Evaluation of Impact Reduction

1) Evaluation Method of Impact Reduction: The purposes of this experiment is to confirm that the preemptive impact reduction method is effective and independent of reflectance. Therefore, the impedance control part is replaced with the position controller implemented in the motor driver (the position mode), based on the results of Section III-B for evaluation independent of the effect of contact impedance control.

The situation in this experiment was equivalent to that shown in Fig. 3(c). The obstacle approached with a constant velocity of -0.3 m/s using the velocity mode of the motor driver. After establishing contact, the mode of manipulating the obstacle was switched to force mode with a force command of 0 N, denoting that friction was the only resistance to moving the obstacle. The plant's desired location x_d was set to 0 m. The collision was performed three times for each object shown in Fig. 5. The control parameters in this experiment are shown in Table II.

2) Evaluation Results of Impact Reduction: Fig. 6 shows the behavior of impact reduction. When the obstacle was nearby, the plant backed away from it. When the obstacle reached the plant, the plant forced the obstruction to return to its starting point because f_p turned to 0. The behavior during the return back to the origin corresponds to the free vibration of the virtual object as determined in the admittance control part of the operation.

The impact force measurements are shown in Table III . Note that the maximum force sensor output is the impact force.

TABLE III
IMPACT REDUCTION EFFECTS WHEN OBSTACLES OF DIFFERENT COLORS APPROACHED

	No reduction ($G_\mathrm{p} = 0.00$)	White	Gray1	Gray2	Gray3	Yellow	Blue	Red	Green
Reflectance ratio to White (%)	-	100	76.5	54.1	30.0	81.3	78.7	76.8	63.3
Impact reduction effect ratio to White (%)	0.00	100	98.0	94.5	81.2	96.3	97.0	96.7	97.1
Impact reduction effect (%)	0.00	75.1	73.6	71.0	61.0	72.4	72.9	72.7	72.3
Ratio of impact force (%)	100	24.9	26.4	29.0	39.0	27.6	27.1	27.3	27.0
Mean value of impact force (N)	15.3	3.81	4.04	4.44	5.97	4.23	4.15	4.19	4.14
SD of impact force (N)	0.0553	0.145	0.115	0.0671	0.266	0.0818	0.0451	0.0538	0.115
The first impact force (N)	15.3	3.61	4.02	4.35	5.60	4.30	4.20	4.22	3.98
The second impact force (N)	15.3	3.88	3.90	4.45	6.07	4.28	4.09	4.23	4.21
The third impact force (N)	15.4	3.94	4.19	4.51	6.23	4.12	4.17	4.11	4.23

TABLE IV
IMPACT REDUCTION EFFECTS OF CONTACT IMPEDANCE CONTROL ONLY AND THE PROPOSED METHOD

Controller	Contact impedance control only (**CI**) ($G_\mathrm{p} = 0.00$)		The proposed method ($G_\mathrm{p} = 0.80$)	
Obstacle velocity (m/s)	-0.3	-0.4	-0.3	-0.4
Impact reduction effect ratio to no reduction shown in Table III (%)	17.9	-	76.8	-
Ratio of impact force to no reduction shown in Table III (%)	82.1	-	23.2	-
Impact reduction effect ratio to **CI** (%)	0.00	0.00	71.7	74.1
Ratio of impact force to **CI** (%)	100	100	23.2	25.9
Mean value of impact force (N)	12.6	17.5	3.56	4.53
SD of impact force (N)	0.0687	0.0410	0.0988	0.155
The first impact force (N)	12.5	17.5	3.65	4.40
The second impact force (N)	12.6	17.5	3.61	4.75
The third impact force (N)	12.6	17.6	3.42	4.45

It is confirmed that the peak outputs occurred immediately after contact.

When $G_\mathrm{p} = 0$, i.e., the impact reduction was disabled, the mean value of the impact force was 15.3 N. The mean values of the impact force were 3.81–5.97 N when preemptive impact reduction was enabled. The impact reduction effect was 61.0–75.1%, where the impact reduction effect was calculated as follows: $100\times$[(the mean without reduction) $-$ (the mean of the case)]/(the mean without reduction).

Moreover, the impact reduction effect ratios were computed by normalizing with the impact reduction effect for the white color to confirm the relationship between reflectance and the reduction effect. The reflectance ratio was calculated by dividing each proximity sensor's output during contact by the output for white. Fig. 7 shows this relationship.

According to Fig. 7, reflectance has no influence on the impact reduction effect. The difference in the decrease impact was only 5.5 % even though Gray2 had a reflectance that was half that of white. Gray3 reduces the reduction effect, nevertheless, to 81.3%. The drop results from the calibration being insufficient. Although the proximity sensor cannot detect any obstacles, there is a very faint signal in the output after calibration. Let ε represent the weak signal and ξ denote the sensor output resulting from obstacle detection. In this scenario, the virtual viscous force can be expressed as $G_\mathrm{p}\dot{\xi}/(\xi+\varepsilon)$. If $\xi \gg \varepsilon$, ε is negligible, yielding $G_\mathrm{p}\dot{\xi}/(\xi+\varepsilon) \approx G_\mathrm{p}\dot{\xi}/\xi$. Alternatively, if ε dominates, it suppresses the virtual viscous force, leading to $|G_\mathrm{p}\dot{\xi}/(\xi+\varepsilon)| < |G_\mathrm{p}\dot{\xi}/\xi|$. Ultimately, the impact reduction performance is impaired. Unlike the reflectance problem, this problem can be solved by increasing the amount of light emitted or the sensitivity of the sensor.

C. Evaluation of Smooth Transition

1) Evaluation Method of Smooth Transition: This experiment was conducted to ensure that impact reduction is not limited by contact impedance control and that the transition from impact reduction to contact impedance control is seamless.

First, the collision shown in Fig. 3(c) was executed. The obstacle velocity was set to -0.3 m/s for comparison with Section IV-B and -0.4 m/s to examine the influence of different obstacle velocities.

The experiment was then performed under the scenario depicted in Fig. 3(d). The plant followed the desired state and ran into the roadblock placed in its path. The trajectory planner

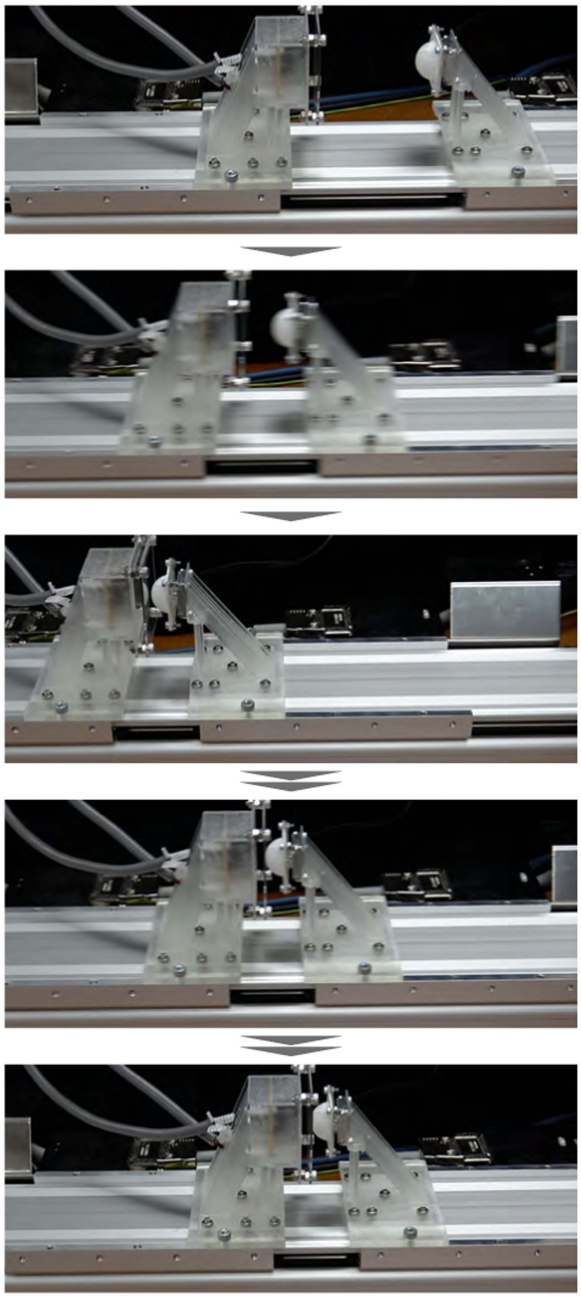

Fig. 6. Behavior of impact reduction when the obstacle approached the plant. The preemptive movement occurred by virtual viscous force. After contact, the plant returned to its origin because the virtual viscous force became zero.

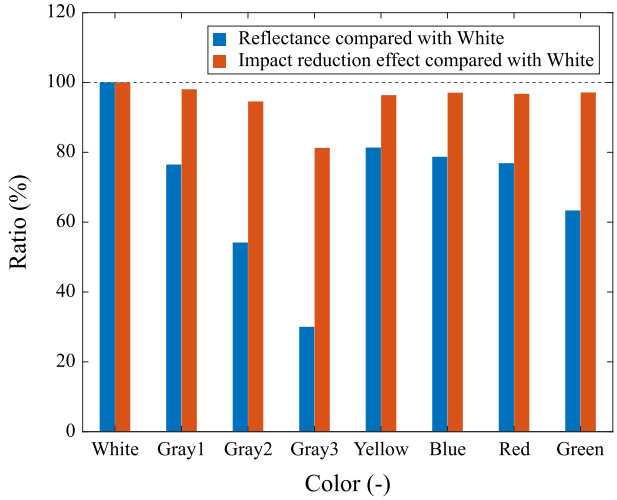

Fig. 7. Relationship between reflectance and the impact reduction effect. The differences in the impact reduction effect are less than those in the reflectance.

generated the desired state trajectory to be a minimum jerk trajectory.

In these experiments, the only color of the obstacle was white. The impedance control part was implemented using (21), and the control settings were established as stated in Table II. We note that m was decided from the datasheet of the dual linear stage, and $\zeta_{\mathrm{i}} = 1$ and $\omega_{\mathrm{i}} = 3\omega_{\mathrm{a}}$ such that ω_{a}, ζ_{i}, and ω_{i} satisfy (37).

2) Evaluation Results of Smooth Transition: Table IV shows the results where the obstacle approached the plant. When the obstacle velocity was -0.3 m/s, the mean value of the impact force was 12.6 N when $G_{\mathrm{p}} = 0$: This indicates that by utilizing contact impedance control only (abbreviated as **CI**), the impact force is decreased. As per Section IV-B, the impact reduction effect ratio to no reduction was 17.9 %. The average impact force was 3.56 N when using the proposed method: combining the preemptive impact reduction and contact impedance control. The impact reduction effect ratio to no reduction shown in Section IV-B was 76.8%, and that to **CI** was 71.7 %. These results indicate that the combination of preemptive impact reduction and contact impedance control is adequate for impact reduction. Preemptive impact reduction only, as indicated in Section IV-B, and **CI** both had lower effects than the combined controller.

When the obstacle velocity was -0.4 m/s, the mean value of the impact force was 17.5 N for **CI**, whereas it was 4.53 N with the proposed method. The impact reduction effect ratio to **CI** was 74.1%. This result shows that the effect of impact reduction was equal to or greater than that recorded with a velocity of -0.3 m/s.

Fig. 8 shows the plant's positional trajectory when it followed the desired state. When there was no barrier, the plant continued along the minimum jerk trajectory that was assigned. When the trajectory encountered a fixed obstacle, the plant collided and came to a stop. Before the accident, the plant was slowed by the proximity sensor's impact reduction. We note that since the results of the three trials were almost the same, the figure depicts only one of each.

The measured contact forces are shown in Fig. 9. We note that the horizontal axis scale is different from that in Fig. 8. The peak of the impact force was 13.6 N for **CI**, whereas it was 2.08 N with the proposed method. The impact reduction effect ratio to **CI** was 84.7%. Moreover, in the case where the proposed method is used, the contact force gradually increased, as shown analytically in Section III-C. No undesired contact force was present immediately following the incident. The length of the transition is determined by ω_{a}. This outcome demonstrated that the transition from impact reduction to contact impedance control is smooth.

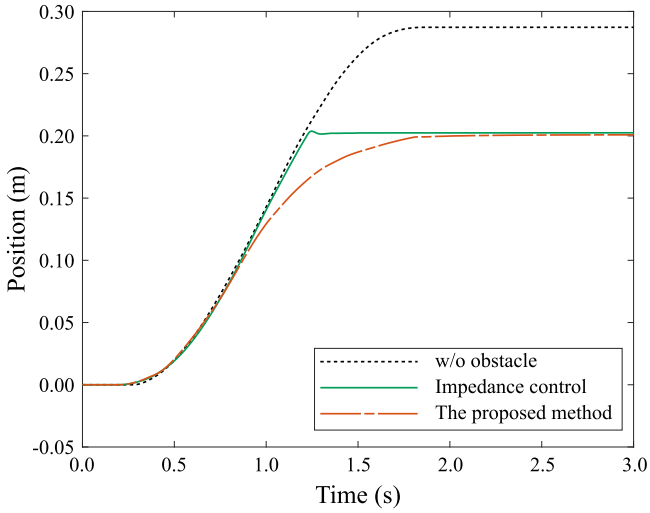

Fig. 8. Position trajectories of the plant when it followed the intended course. The differences in these trajectories were brought about by the fixed obstacle and preemptive impact reduction feature.

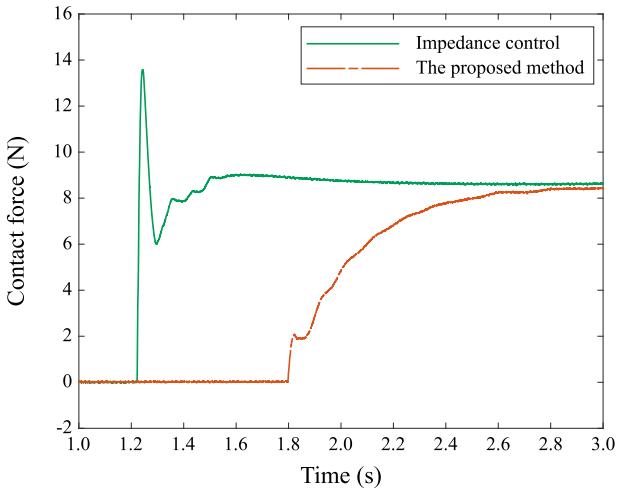

Fig. 9. Measured contact force that occurred when the plant hit the fixed obstacle on the path. Each impact force is shown by the first peak of each wave. Before convergence in the outcome, when the preemptive impact reduction was enabled, there was no peak other than the impact force.

V. Expansions

A. Proposed Controller for Position/Velocity-Control-Based Robots

Fig. 10 shows the proposed controller for position/velocity-control-based robots. The second admittance control part and the position/velocity controller are used in place of the impedance control part in contrast to Fig. 1. In the following, the controller shown in Fig. 1 is referred to as proximity admittance and contact impedance controller (PACIC), whereas the controller shown in Fig. 10 is referred to as proximity admittance and contact admittance controller (PACAC).

In the PACAC, (2) is replaced with

$$M_{\mathrm{a},1}(\ddot{x}_{\mathrm{v},1}-\ddot{x}_{\mathrm{d}})+D_{\mathrm{a},1}(\dot{x}_{\mathrm{v},1}-\dot{x}_{\mathrm{d}})+K_{\mathrm{a},1}(x_{\mathrm{v},1}-x_{\mathrm{d}})=f_{\mathrm{p}} \tag{39}$$

where the subscripts are expanded from each. The following equation and any position/velocity controller are used instead of (4)

$$M_{\mathrm{a},2}\left(\ddot{x}_{\mathrm{v},2}-\ddot{x}_{\mathrm{v},1}\right)+D_{\mathrm{a},2}\left(\dot{x}_{\mathrm{v},2}-\dot{x}_{\mathrm{v},1}\right) + K_{\mathrm{a},2}(x_{\mathrm{v},2}-x_{\mathrm{v},1})=f_{\mathrm{c}}. \tag{40}$$

By replacing (2) with (39) and (5) with (40), the same analysis results as in Sections III-B and III-C are obtained. The characteristic difference between PACIC and PACAC is similar to the distinction between conventional impedance and admittance control mentioned in Section I-B1.

B. Generalized Serial Combined Impedance Controller

Fig. 11 shows the generalized controller, including the controller proposed in [17], the PACIC, and the PACAC. There are N admittance control parts, as well as either an additional admittance control part or an impedance control part. Virtual or contact force sensor outputs are received by each admittance control part. The following part's desired state is based on each output of the admittance control part. Each admittance control part determines the influence of the related sensor output on its target state, as discussed in Section III-B. We note that delays may occur depending on the control parameters. Such stacked delays will undermine the performance of the control.

The controller proposed in [17] has an admittance control part and an impedance control part, and the admittance control part receives a contact force sensor output. Namely, in the PACIC and the PACAC, two control parts are connected through the virtual object's state, whereas in the controller presented in [17], they are also connected through force. This distinction allows for drastically different controller characteristics from the one given in this study, i.e., the generalized controller may be widely applicable. The characteristics in the case of [17] are further investigated in [26].

VI. Discussion

A. Example of the Design Process

An example of the design process of the proposed controllers is shown as follows.

1) *Parameter design for contact impedance control:* We design the parameters for either the impedance control part or the second admittance control part, as proposed in Section II or Section V-A according to a given task. Nothing needs to be changed if contact impedance/admittance control has been implemented.
2) *Parameter design for smooth transition:* The parameters of the admittance control part receiving virtual viscous force are designed so that (38) is satisfied and $\zeta_{\mathrm{a}}=1$. A parameter design with some margin for tolerance is recommended.
3) *Gain tuning for impact reduction:* We find a suitable value of G_{p} in (1) for impact reduction in an ad hoc process. The systematic design method needs to be developed in future work.

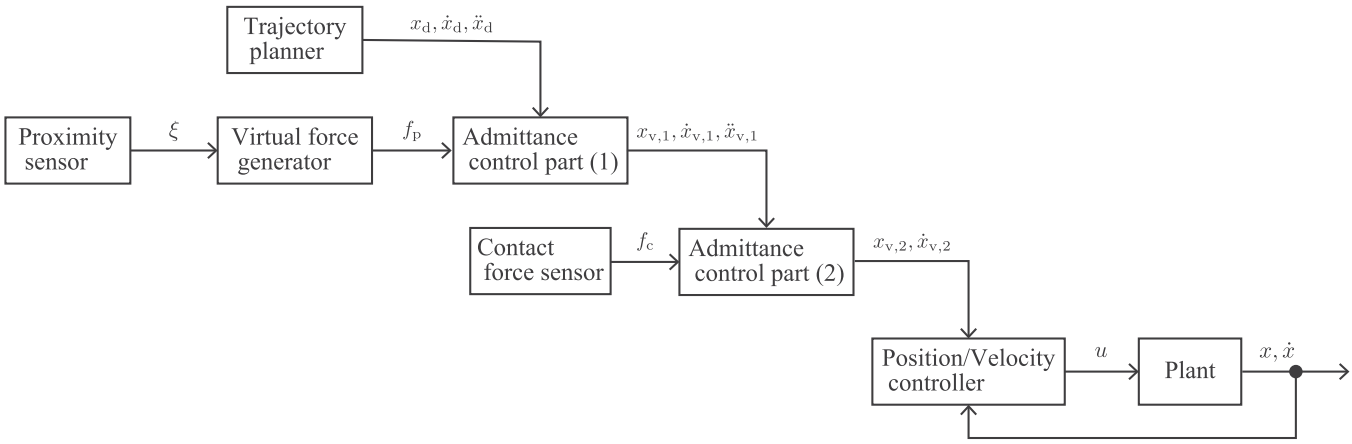

Fig. 10. Block diagram of the proposed controller for position/velocity-control-based robots. There are two admittance control parts. The first is for virtual force, whereas the other is for contact force. The output of the first admittance control part serves as the second admittance control part's desired state.

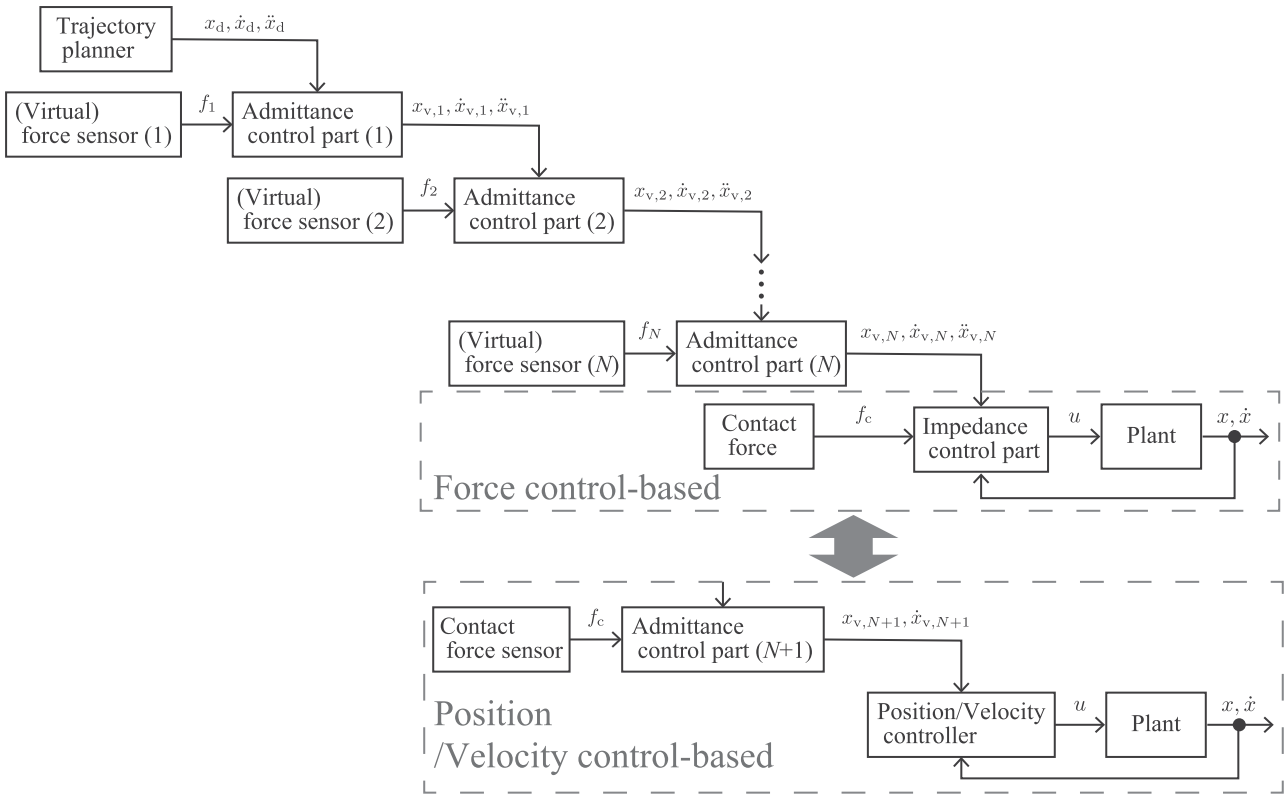

Fig. 11. Generalized serial combined impedance controller is shown in a block diagram. As with the controller in [17], the same virtual or contact force can also serve as the input for several admittance control parts. Depending on the plant's control type, the last part should be chosen.

B. Limitations

An inherent limitation of the proposed method is that it requires a proximity sensor. As stated in [12], it is difficult to incorporate a proximity sensor in the contact area. However, a simple optical proximity sensor is sufficient for the proposed method. Due to their small size, simple optical proximity sensors can be mounted in tight spaces or used to cover contact areas. Some related examples exist, such as mounting on a fingertip [27], on a tiptoe [11], on feet [12], and covering a robot arm [28]. In addition, high-density implementation is feasible, as presented in [29], and enhances the signal-to-noise ratio described in Section IV-B. Intelligent proximity sensors that measure distance, such as a time-of-flight sensor IC (VL6180X, STMicroelectronics N.V., Geneva, Switzerland), which have become popular in recent years, or a bespoke sensor [21] can also be utilized in the suggested technique in place of simple proximity sensors. The virtual viscous force can be derived by differentiating the distance output, as proposed in [21]. Because the admittance control part functions as a reliable second-order

filter, it should be noted that even though the differentiator generally amplifies high-frequency noise, the influence of the noise on plant motion is minimal in the proposed method, as demonstrated by the experimental results. When the sensor output is minute, signifying the absence of obstacles, the amplified high-frequency noise may only be partially eliminated in some environments. Substituting f_{p}, e.g., $f_{\mathrm{p}} = 0$ when $\xi \approx 0$, is an example of a practical solution in this scenario. Although this approach may render f_{p} discontinuous, the plant's motion remains continuous because of the functionality of the admittance control part. Other forces that satisfy the analysis's presumption that $f_{\mathrm{p}} = 0$ in contact can be used in place of the virtual viscous force. For instance, the virtual elastic force is suitable to the suggested method when using the sensor design method given in [11]. Other virtual forces obtained by other types of proximity sensors may also be utilized in conjunction with the proposed method as long as they satisfy the above assumptions. For example, capacitive proximity sensors may prove advantageous in detecting obstacles that are difficult to detect with optical sensors.

The plant in this article is only a 1-D mass model. The example of the application method mentioned in Section I-C is merely one possible candidate. Future research to adapt the proposed method to complex systems will build upon the contributions of this article. Significantly, even in forthcoming investigations, analyzing the approaching direction is an imperative topic in any discussion of collisions. Therefore, the findings of this study will be useful for subsequent work.

C. (Byproduct) Contact Preservation

The contact state can also be maintained by the virtual viscous force when the transition from contact to noncontact is likely to occur. For specific tasks, such as keeping a grabbed object from being dropped from a robot hand, this functionality would be useful. Future studies will evaluate contact preservation according to defined tasks. We note that if it is not necessary to preserve contact, you can disable the contact preservation feature by using saturation.

VII. Conclusion

This article introduced novel control methods that reduce the impact and control contact force after a collision. One of the techniques is for force-control-based robots and uses a virtual viscous force generator, an admittance control part, and an impedance control part. Another employs the second admittance control part for contact force instead of the previously described impedance control part and is for position/velocity-control-based robots.

The related analyses and experiments demonstrated three advantages. The first is that even though the impact reduction technique uses a simple optical proximity sensor to react before contact, the effect of reflectance on impact reduction is negligible. Despite a small influence of the experiment's insufficient calibration, the analytical outcome shows that the feature is independent of reflectance, provided that the obstacle is detectable. The second advantage is that impact reduction and contact impedance control can be accomplished separately by designing the control parameters according to a given task. Preemptive impact reduction is easily added; if contact impedance control is already in place, its parameters do not need to be altered. In the experiments, adding the preemptive impact reduction reduced the impact force by 71.7% when the obstacle approached the plant and by 84.7% when the plant approached the fixed obstacle. The third advantage is the smooth transition from impact reduction to contact impedance control. Both switching and unwelcome contact forces are absent. The contact impedance control is gradually enabled. The majority of robots that need to interact with environments, objects, and humans can benefit from these advantages.

References

[1] R. Alexander, "Three uses for springs in legged locomotion," *Int. J. Robot. Res.*, vol. 9, no. 2, pp. 53–61, 1990.

[2] J. J. Rond, M. C. Cardani, M. I. Campbell, and J. W. Hurst, "Mitigating peak impact forces by customizing the passive foot dynamics of legged robots," *J. Mech. Robot.*, vol. 12, no. 5, 2020, Art. no. 051010.

[3] G. De Magistris, S. Miossec, A. Escande, and A. Kheddar, "Design of optimized soft soles for humanoid robots," *Robot. Auton. Syst.*, vol. 95, pp. 129–142, 2017.

[4] A. Pajon, S. Caron, G. De Magistri, S. Miossec, and A. Kheddar, "Walking on gravel with soft soles using linear inverted pendulum tracking and reaction force distribution," in *Proc. Int. Conf. Humanoid Robot.*, 2017, pp. 432–437.

[5] J. H. Park and H. Chung, "Hybrid control for biped robots using impedance control and computed-torque control," in *Proc. Int. Conf. Robot. Autom.*, 1999, vol. 2, pp. 1365–1370.

[6] C. Ott, A. Albu-Schaffer, A. Kugi, and G. Hirzinger, "On the passivity-based impedance control of flexible joint robots," *IEEE Trans. Robot.*, vol. 24, no. 2, pp. 416–429, Apr. 2008.

[7] S. K. Au, J. Weber, and H. Herr, "Powered ankle–foot prosthesis improves walking metabolic economy," *IEEE Trans. Robot.*, vol. 25, no. 1, pp. 51–66, Feb. 2009.

[8] A. Lecours, B. Mayer-St-Onge, and C. Gosselin, "Variable admittance control of a four-degree-of-freedom intelligent assist device," in *Proc. Int. Conf. Robot. Autom.*, 2012, pp. 3903–3908.

[9] F. Ficuciello, L. Villani, and B. Siciliano, "Variable impedance control of redundant manipulators for intuitive human–robot physical interaction," *IEEE Trans. Robot.*, vol. 31, no. 4, pp. 850–863, Aug. 2015.

[10] W. Huo et al., "Impedance modulation control of a lower-limb exoskeleton to assist sit-to-stand movements," *IEEE Trans. Robot.*, vol. 38, no. 2, pp. 1230–1249, Apr. 2022.

[11] R. Sato, H. Arita, and A. Ming, "Pre-landing control for a legged robot based on tiptoe proximity sensor feedback," *IEEE Access*, vol. 10, pp. 21619–21630, 2022.

[12] J. R. Guadarrama-Olvera, S. Kajita, and G. Cheng, "Preemptive foot compliance to lower impact during biped robot walking over unknown terrain," *IEEE Robot. Autom. Lett.*, vol. 7, no. 3, pp. 8006–8011, Jul. 2022.

[13] S. E. Navarro et al., "Proximity perception in human-centered robotics: A survey on sensing systems and applications," *IEEE Trans. Robot.*, vol. 38, no. 3, pp. 1599–1620, Jun. 2022.

[14] N. Hogan, "Impedance control—Part 1—part 3," *Trans. ASME J. Dyn. Syst. Meas. Control*, vol. 107, pp. 1–24, 1985.

[15] K. Kosuge, K. Furuta, and T. Yokoyama, "Mechanical impedence control of a robot arm by virtual internal model following controller," *IFAC Proc. Vol.*, vol. 20, no. 5, pp. 239–244, 1987.

[16] C. Ott, R. Mukherjee, and Y. Nakamura, "A hybrid system framework for unified impedance and admittance control," *J. Intell. Robot. Syst.*, vol. 78, no. 3, pp. 359–375, 2015.

[17] T. Fujiki and K. Tahara, "Numerical simulations of a novel force controller serially combining the admittance and impedance controllers," in *Proc. Int. Conf. Robot. Autom.*, 2021, pp. 6955–6962.

[18] T. Tsuji and M. Kaneko, "Noncontact impedance control for redundant manipulators," *IEEE Trans. Syst., Man, Cybern. A, Syst. Humans*, vol. 29, no. 2, pp. 184–193, Mar. 1999.

[19] S.-Y. Lo, C.-A. Cheng, and H.-P. Huang, "Virtual impedance control for safe human-robot interaction," *J. Intell. Robot. Syst.*, vol. 82, no. 1, pp. 3–19, 2016.
[20] G. Cheng, E. Dean-Leon, F. Bergner, J. R. G. Olvera, Q. Leboutet, and P. Mittendorfer, "A comprehensive realization of robot skin: Sensors, sensing, control, and applications," *Proc. IEEE*, vol. 107, no. 10, pp. 1–18, Oct. 2019.
[21] K. Koyama, K. Murakami, T. Senoo, M. Shimojo, and M. Ishikawa, "High-speed, small-deformation catching of soft objects based on active vision and proximity sensing," *IEEE Robot. Autom. Lett.*, vol. 4, no. 2, pp. 578–585, Apr. 2019.
[22] K. Koyama, Y. Suzuki, A. Ming, and M. Shimojo, "Grasping control based on time-to-contact method for a robot hand equipped with proximity sensors on fingertips," in *Proc. Int. Conf. Intell. Robot. Syst.*, 2015, pp. 504–510.
[23] H. Arita and Y. Suzuki, "Contact transition control by adjusting emitting energy of proximity sensor," *Adv. Robot.*, vol. 35, no. 2, pp. 93–107, 2021.
[24] Y. Ding and U. Thomas, "Improving safety and accuracy of impedance controlled robot manipulators with proximity perception and proactive impact reactions," in *Proc. Int. Conf. Robot. Autom.*, 2021, pp. 3816–3821.
[25] Y. Ding and U. Thomas, "Collision avoidance with proximity servoing for redundant serial robot manipulators," in *Proc. Int. Conf. Robot. Autom.*, 2020, pp. 10249–10255.
[26] T. Fujiki and K. Tahara, "Series admittance–impedance controller for more robust and stable extension of force control," *Robomech J.*, vol. 9, no. 1, 2022, Art. no. 23.
[27] A. R. Johnston, "Optical proximity sensors for manipulators," Jet Propulsion Lab., Pasadena, CA, USA, Tech. Rep. JPL-TM-33-612, 1973.
[28] E. Cheung and V. Lumelsky, "Development of sensitive skin for a 3D robot arm operating in an uncertain environment," in *Proc. Int. Conf. Robot. Autom.*, 1989, vol. 2, pp. 1056–1061.
[29] Y. Suzuki, "Proximity-based non-contact perception and omnidirectional point-cloud generation based on hierarchical information on fingertip proximity sensors," *Adv. Robot.*, vol. 35, no. 20, pp. 1181–1197, 2021.

Hikaru Arita (Member, IEEE) received the bachelor's, master's, and doctoral degrees in engineering from the University of Electro-Communications, Tokyo, Japan, in 2012, 2014, and 2019, respectively.

He served several institutions, including OMRON Corporation, Kyoto, Japan, where he worked from 2014 to 2016, and Ritsumeikan University, where he was an Assistant Professor from 2019 to 2022. He is currently an Assistant Professor with Kyushu University, Fukuoka, Japan. His research interests include proximity sensors and sensor-based control.

Hayato Nakamura received the bachelor's degree in engineering in 2022 from Kyushu University, Fukuoka, Japan, where he is currently working toward the master's degree in engineering.

His research interests include the control of robots using proximity sensors.

Takuto Fujiki received the bachelor's, master's, and doctoral degrees in mechanical engineering from Kyushu University, Fukuoka, Japan, in 2018, 2020, and 2023, respectively.

He is currently with Yaskawa Electric Corporation, Fukuoka, Japan. His major is mechanical engineering and his area of expertise is control engineering. His main research interests include force control that combines multiple force controls.

Kenji Tahara (Member, IEEE) received the B.S. degree in mechanical engineering, the M.S. degree in information science and systems, and the Ph.D. degree in robotics from Ritsumeikan University, Japan, in 1998, 2000, and 2003, respectively.

From 2003 to 2007, he was a Research Scientist with the Bio-Mimetic Control Research Center, RIKEN, Japan. In 2007, he joined Kyushu University, Fukuoka, Japan, as a tenure-track Associate Professor. In 2011, he was an Associate Professor with the Department of Mechanical Engineering, Kyushu University, where he has been a Full Professor since 2020. His current research interests include mechanics, design, and control of multifingered robotic hands, soft robotics including polymeric artificial muscle actuators, force control, bipedal robots, and analysis and realization of human body movements.